

# Silver Contact Grid: Inferred Contact Resistivity and Cost Minimization in 19% Silicon Solar Cells

Daniel L. Meier, *Member, IEEE*, Vinodh Chandrasekaran, *Member, IEEE*, Atul Gupta, Vijay Yelundur, and Ajeet Rohatgi, *Fellow, IEEE*

**Abstract**—The analysis of silicon solar cell contacts having an H-bar front grid pattern is extended by enabling the contact resistivity to be inferred from the measurement of total series resistance and the determination of six individual components of series resistance. Analysis of the contact system was completed for a representative 19% cell fabricated from a 156-mm pseudosquare p-Cz wafer using standard production processes, including phosphorus ion implantation, thermal oxide surface passivation, silicon nitride deposition, and screen-printing and firing of front silver gridlines and busbars, back silver soldering pads, and back aluminum contact. Gridline width was measured to be 80  $\mu\text{m}$  after firing, with an average thickness of 7.4  $\mu\text{m}$  and an effective resistivity of 4.7  $\mu\Omega\cdot\text{cm}$ . Contact resistivity to the uniform 91  $\Omega/\square$  emitter was inferred to be 5.3  $\text{m}\Omega\cdot\text{cm}^2$  from the total series resistance and its components. Using these values, gridline spacing was optimized for maximum efficiency (1.7 mm, 91 lines, 19.1%, \$0.040/W) or minimum silver cost (2.1 mm, 74 lines, 19.0%, \$0.038/W). The analysis methodology was further applied to examine the impact of gridline width and silver pricing on cell efficiency and incremental cost. Such analysis can serve as a guideline for future contact system designs when the cost of silver changes or when printing technology allows narrower lines.

**Index Terms**—Contacts, silicon, silver, solar energy.

## I. INTRODUCTION

**N**EXT to the silicon wafer itself, the contact materials are the most costly element of crystalline silicon solar cells in production today. The most common materials are silver for the front grid and back soldering pads, and aluminum for the back contact. These are usually deposited by screen printing and then co-fired in a belt furnace. Silver is a popular choice for the front grid because of its high electrical conductivity, solderability, and long-term stability. Silver particles can readily be incorporated into a screen-printable paste along with proprietary components, such as glass frit, binders, and solvents. These enable the printing

of narrow, yet reasonably tall lines, which can be fired through front dielectric layers to contact the doped front silicon surface of the solar cell with low contact resistance. However, silver is also a costly material (approximately \$1/g), and therefore efforts are made to minimize its use. A front grid system is often designed to maximize cell efficiency, with grid shadowing balanced against ohmic losses, but it is perhaps more important from a commercial viewpoint to minimize the incremental cost ( $\Delta\$/\text{W}$ ) of the silver grid. Toward that end, this paper has the following objectives.

- 1) Provide a complete and updated set of expressions to calculate the normalized components of series resistance ( $\Omega\cdot\text{cm}^2$ ) in a modern large-area silicon solar cell with an “H-bar” front contact pattern of parallel grid lines and perpendicular busbars.
- 2) Provide a means for inferring silver/silicon contact resistivity without having to resort to a current transfer length method (TLM) measurement.
- 3) Apply the analysis techniques to cells fabricated with state-of-the-art production processes to optimize the grid pattern for minimum incremental cost ( $\Delta\$/\text{W}$ ).
- 4) Calculate, based on measured cell values, the optimal gridline spacing required for maximum efficiency or for minimum  $\Delta\$/\text{W}$  with gridline width and silver cost as parameters.

Analysis is carried out with cells fabricated using standard production processes at Suniva. Cells begin with a textured (both sides) p-Cz wafer and feature a uniform ion-implanted phosphorus front emitter, thermal silicon dioxide surface passivation, silicon nitride antireflective coating, aluminum back surface field, front silver grid, and back silver soldering pads.

## II. EXPRESSIONS FOR SERIES RESISTANCE COMPONENTS

An early treatment of the front contact for large area (100-mm square) solar cells is given in [1]. Of the four grid patterns considered, the one with the lowest total power loss was an H-bar design with parallel grid lines and four orthogonal busbars. The pattern had a 6.1% shadowing loss and a 1.4% ohmic ( $J_{\text{mp}}^2 * R_{\text{series}}$ ) loss for a total loss of 7.5%. These values were obtained with copper grid lines having a width of 75  $\mu\text{m}$ , a thickness of 10  $\mu\text{m}$ , and a spacing of 2.0 mm. The four busbars were copper wires, each 0.644 mm in diameter. The copper grid contacted an emitter layer having 35  $\Omega/\square$  sheet resistance, and the base was 200  $\mu\text{m}$  thick with 1  $\Omega\cdot\text{cm}$  resistivity. Other treatments of contact systems can be found in [2]–[4], including consideration of an H-bar design with an arbitrary number of busbars.

Manuscript received July 13, 2012; revised August 24, 2012; accepted August 27, 2012. Date of publication October 9, 2012; date of current version December 19, 2012.

D. L. Meier was with Suniva, Norcross, GA 30092 USA. He is now with Lightdrop Harvest, LLC, St. Marys, PA 15857 USA (e-mail: dmeier@lightdropharvest.com).

V. Chandrasekaran, A. Gupta, V. Yelundur, and A. Rohatgi are with Suniva, Norcross, GA 30092 USA (e-mail: vchandrasekaran@suniva.com; agupta@suniva.com; vyelundur@suniva.com; arohatgi@suniva.com).

A. Rohatgi is with Suniva, Norcross, GA 30092 USA, and also with the University Center of Excellence for Photovoltaics, Georgia Institute of Technology, Atlanta GA 30332 USA (e-mail: ajeet.rohatgi@ece.gatech.edu).

Color versions of one or more of the figures in this paper are available online at <http://ieeexplore.ieee.org>.

Digital Object Identifier 10.1109/JPHOTOV.2012.2217939

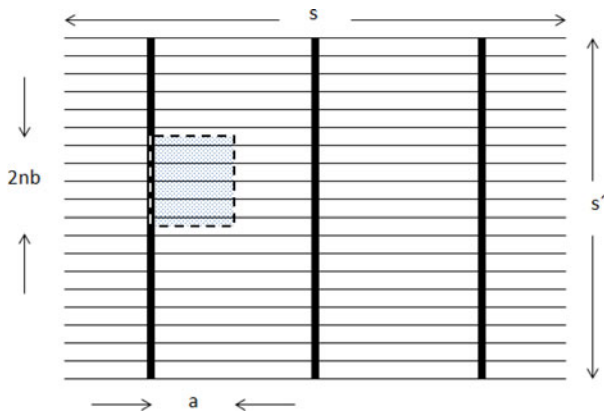


Fig. 1. Diagram of rectangular H-bar pattern with three busbars. Subcell used for analysis has length  $a = s/(2n_{bb}) = s/6$  and width  $2nb$ , where  $2b$  is center-to-center spacing between gridlines, and  $2nb$  is the spacing between current pick-up probes in the cell tester.

Basic expressions for calculating the power loss from different regions of the solar cell are derived in [5] for a “comb” grid pattern (grid lines perpendicular to a single busbar). Building on these expressions, the components of series resistance (normalized to unit cell area) are developed in [6] for a two-bus H-bar pattern. This paper treats a more general H-bar pattern applied to a rectangular cell with any number of busbars, and also includes an updated expression for the series resistance component associated with the front busbar. Shown in Fig. 1, for example, is a rectangular cell with three busbars, typical of cells currently in production. The key construct is an elementary subcell “ $a$ ” units long and “ $2nb$ ” units wide, with “ $n$ ” grid lines having center-to-center spacing of “ $2b$ ” units. Current pick-up probes in a cell tester are assumed to have a spacing equal to the subcell width ( $2nb$ ). For a full cell “ $s$ ” units long, the length of the subcell ( $a$ ) is  $s/(2n_{bb})$ , where  $n_{bb}$  is the number of busbars. For example, a production cell 156 mm long with three busbars will be represented by a subcell of length 26 mm. The arrangement in Fig. 1 shows five gridlines per subcell, which is representative for typical current probe separation. However, it should be noted that the formalism is accurate, even if  $n$  is not an integer.

There is usually a disconnect between analytical grid design and actual implementation on a cell. This is because the analysis assumes uniform gridlines having constant width and thickness (rectangular cross-section) and a constant and known resistivity. In practice, the cross section is not rectangular, and neither the width nor the thickness is constant—particularly for screen-printed lines. This is shown in Fig. 2 by the 3-D image of a grid line, taken with a digital microscope (Keyence VHX-600). The observed undulations result from paste being squeezed through the mesh of wires in the screen. Furthermore, the resistivity of the grid line is not necessarily the handbook value for bulk material. For example, a screen-printed silver line is made up of silver particles which are sintered together. Proprietary materials in the silver paste (organic binders, glass frit) may introduce some resistance between the sintered silver particles, thereby increasing the effective resistivity of the line. In addition, small

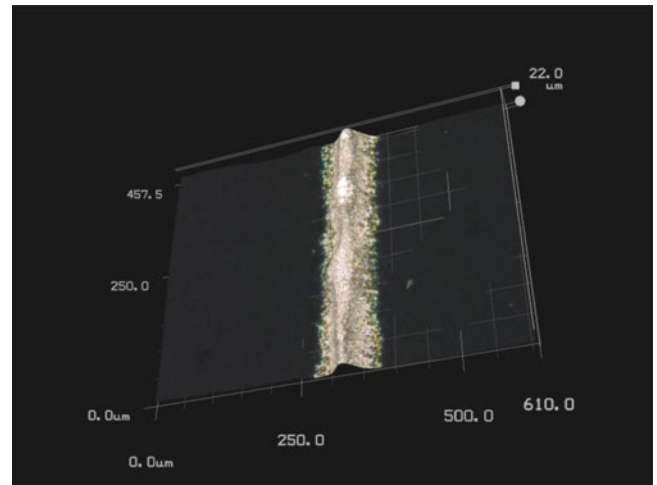


Fig. 2. Three-dimensional microscope image of a screen-printed silver gridline showing nonuniformity in both thickness and width, with peak thickness of  $22 \mu\text{m}$  (Suniva cell LDE-G3-17).

voids exist within the line—again increasing its effective resistivity.

In the analysis described here, complications associated with nonuniformity of gridline width  $w$ , thickness  $t$ , and resistivity  $\rho$  are avoided by recognizing that the individual values of  $w$ ,  $t$ , and  $\rho$  are not needed, but only the combination  $\rho/(tw)$  is needed. This combination can be easily determined empirically from a cell by the measurement of resistance between adjacent busbars, which is a measurement of the parallel combination of all  $n_{gl}$  gridline segments between the two busbars. The measurement is called “busbar-to-busbar resistance” (BBR) and provides an effective value of the required combination of  $\rho/(tw)$ , averaged over all  $n_{gl}$  gridlines. A similar value for the combination of parameters required for the busbar  $\rho/(tw)$  is obtained by the measurement of the resistance of the full length of the physical busbar on the cell. Here, recognize that  $w$  is the width of the busbar in the subcell, which is half the width of the physical busbar of the cell, as shown in Fig. 1. Thus, two simple measurements on the finished cell (BBR and busbar resistance) provide the information needed to calculate the series resistance components associated with the gridlines and with the front busbar. No corrections are made to these measured values for front contact resistance or emitter sheet resistance, as such corrections alter the measured resistance values of the metal gridlines and busbars insignificantly. The individual components of series resistance, normalized to unit area, can now be quantified with convenient units of  $\Omega\cdot\text{cm}^2$ .

The expressions used to calculate six components of series resistance [5], [6] are summarized in Table I.  $R_{bus}$  is the resistance of the front busbar measured over its full length  $s'$  on the finished cell. The expression for  $r_s$  (front busbar) differs from [6] in that  $n^2$  is replaced by  $(n+1)(n+2)$ . This accounts for the fact that current enters the busbar in discrete “lumps,” rather than continuously ( $n^2$ ) as assumed in [6], since each gridline delivers a quantity of current, which then flows along the busbar until it is joined by another “lump” from the next gridline.  $\rho_w$  and  $t_w$  are the resistivity and thickness of the wafer

TABLE I  
EXPRESSIONS FOR CALCULATING NORMALIZED SERIES RESISTANCE COMPONENTS ( $\Omega\text{-cm}^2$ )

| Component    | Expression ( $\Omega\text{-cm}^2$ )   |
|--------------|---|
| Front Busbar | $r_s(\text{front busbar}) = (1/3)a(n+1)(n+2)b^2\rho/(tw') = (1/3)a(n+1)(n+2)b^2(2R_{\text{bus}}/s')$          |
| Gridlines    | $r_s(\text{gridline}) = (2/3)a^2b\rho/(tw) = (1/3)(abn_{\text{gl}})BBR$                                       |
| Front Sheet  | $r_s(\text{sheet}) = (1/3)b^2R_{\text{sheet}}$  |
| Substrate    | $r_s(\text{substrate}) = \rho_w t_w$  |
| Back Metal   | $r_s(\text{back metal}) = (1/3)a^2R_{\text{sheet}}(\text{metal})$   |
| Back Busbar  | $r_s(\text{back busbar}) = r_s(\text{front busbar}) * (\text{width front busbar} / \text{width back busbar})$ |

TABLE II  
MEASURED PARAMETERS FOR CONTACT SYSTEM (CELL LDE2-G3-17)

| Parameter                        | Description  | Value                         |
|----------------------------------|--|-------------------------------|
| s                                | cell horizontal side length                              | 156 mm                        |
| s'                               | cell vertical side length                                | 156 mm                        |
| $n_{\text{bb}}$                  | number of bus bars                                       | 3                             |
| a                                | length of gridlines in subcell                           | 26 mm                         |
| 2b                               | grid line spacing  | 2.10 mm                       |
| n                                | number of gridlines per subcell                          | 5                             |
| $n_{\text{gl}}$                  | total number of gridlines in full cell                   | 74                            |
| w                                | width of gridline  | 80 $\mu\text{m}$              |
| 2w'                              | width of front busbar on cell                            | 1.5 mm                        |
| $R_{\text{sheet}}$               | sheet resistance of front implanted silicon layer        | 91 $\Omega/\square$           |
| $R_{\text{sheet}}(\text{metal})$ | sheet resistance of back metal                           | 7.72 $\text{m}\Omega/\square$ |
| $\rho_w$                         | wafer resistivity  | 2 $\Omega\text{-cm}$          |
| $t_w$                            | wafer thickness (after texturing)                        | 180 $\mu\text{m}$             |
| $J_{\text{sc}}$                  | short circuit current density measured by cell tester    | 37.80 $\text{mA}/\text{cm}^2$ |
| $V_{\text{oc}}$                  | open circuit voltage measured by cell tester             | 0.6410 V                      |
| FF                               | fill factor measured by cell tester                      | 0.7869                        |
| Efficiency                       | efficiency measured by cell tester                       | 19.07%                        |
| PFF                              | pseudo fill factor measured by Suns-Voc                  | 0.830                         |
| BBR                              | busbar-to-busbar resistance                              | 0.056 $\Omega$                |
| $R_{\text{bus}}(\text{front})$   | front busbar resistance                                  | 0.1048 $\Omega$               |
| $w_{\text{back busbar}}$         | width of back busbar (soldering pad)                     | 4.0 mm                        |
| $\Delta\text{FF}/r_s$            | fill factor sensitivity factor (FF loss relative to PFF) | 0.0489/ $\Omega\text{-cm}^2$  |

(substrate).  $R_{\text{sheet}}(\text{metal})$  refers to the sheet resistance of the back metal contact (typically fired aluminum) and represents the loss associated with current traveling to the back busbars. Since the resistance of the back busbar is difficult to measure in a completed cell because of the overlapping aluminum, the (small)  $r_s(\text{back busbar})$  component is approximated by scaling  $r_s(\text{front busbar})$  by busbar widths.

### III. INFERRED CONTACT RESISTANCE COMPONENT OF SERIES RESISTANCE FROM REPRESENTATIVE CELL DATA

Experience has shown that the cell total series resistance, along with the six components of series resistance given in Table I, can be calculated quite accurately and precisely. The total series resistance is determined from the pseudofill factor (PFF), as given by a Suns- $V_{\text{oc}}$  measurement [7], and the cell fill factor (FF) according to the method in [8] as

$$r_s(\text{total}) = [V_{\text{oc}}/J_{\text{sc}}][(\text{PFF} - \text{FF})/\text{PFF}]. \quad (1)$$

Alternatively,  $r_s(\text{total})$  can be determined from measurements of the cell  $I$ - $V$  curves at two different light intensities.

The component of series resistance associated with the front contact resistance can then be inferred by subtracting the sum of the components from the total series resistance. Contact resistivity can, in turn, be determined by multiplying this inferred component by the fractional area covered by the gridlines ( $f$ )

$$r_s(\text{contact}) = r_s(\text{total}) - [r_s(\text{front busbar}) + r_s(\text{gridline}) + r_s(\text{sheet}) + r_s(\text{substrate}) + r_s(\text{back metal}) + r_s(\text{back busbar})] \quad (2)$$

$$\rho_c = [f][r_s(\text{contact})]. \quad (3)$$

Results are summarized in Tables II and III for a 156-mm pseudosquare (239  $\text{cm}^2$  area) Suniva cell with  $J_{\text{sc}}$  of 37.80  $\text{mA}/\text{cm}^2$ ,  $V_{\text{oc}}$  of 0.6410 V, FF of 0.7869, and efficiency of 19.07% (stabilized). A photograph of such a cell is given in Fig. 3. Note that linewidth is 80  $\mu\text{m}$ , and contact is made

TABLE III  
SERIES RESISTANCE COMPONENTS AND INFERRED CONTACT RESISTIVITY (CELL LDE2-G3-17)

| Component                     | Description   | Value                             |
|-------------------------------|---|-----------------------------------|
| $r_s(\text{total})$           | total series resistance of cell (from PFF and FF)       | 0.8806 $\Omega\text{-cm}^2$       |
| $r_s(\text{front busbar})$    | front busbar component                                  | 0.0030 $\Omega\text{-cm}^2$       |
| $r_s(\text{gridline})$        | gridline component                                      | 0.3745 $\Omega\text{-cm}^2$       |
| $r_s(\text{sheet})$           | front sheet component                                   | 0.3281 $\Omega\text{-cm}^2$       |
| $r_s(\text{substrate})$       | substrate component                                     | 0.0360 $\Omega\text{-cm}^2$       |
| $r_s(\text{back metal})$      | back metal component                                    | 0.0174 $\Omega\text{-cm}^2$       |
| $r_s(\text{back busbar})$     | back busbar component                                   | 0.0011 $\Omega\text{-cm}^2$       |
| $\sum r_s(\text{components})$ | (back metal and back busbar not included)               | 0.7416 $\Omega\text{-cm}^2$       |
| $r_s(\text{contact})$         | inferred front contact resistance component             | 0.1390 $\Omega\text{-cm}^2$       |
| f                             | fractional area covered by gridlines                    | 0.0379                            |
| $\rho_c$                      | contact resistivity from inferred $r_s(\text{contact})$ | 5.27 $\text{m}\Omega\text{-cm}^2$ |



Fig. 3. Photograph of 156-mm pseudosquare cell with grid pattern of the type analyzed.

to a 91  $\Omega/\square$  phosphorus-doped emitter (ion implanted and annealed) with a resulting contact resistivity  $\rho_c$  of 5.3  $\text{m}\Omega\text{-cm}^2$ . The phosphorous surface doping concentration is estimated to be  $1.6 \times 10^{20} \text{ P/cm}^3$  based on dopant profiles obtained under similar implant and anneal conditions and measured by the electrochemical  $C$ - $V$  technique. Since the cell FF was determined with a tester having a full metal stage rather than back current probes,  $r_s(\text{back metal})$  and  $r_s(\text{back busbar})$  do not contribute to the total series resistance measured, and so are not included in the calculation of inferred  $r_s(\text{contact})$ . The largest components of series resistance are those from the gridlines, front sheet, and front contact. Overall, shadowing was 6.68% of the cell area and accounted for a power loss of 1.19  $\text{mW/cm}^2$ . Ohmic losses were 0.95  $\text{mW/cm}^2$  or 4.98% of the 19.07% cell efficiency.

The value of  $\rho_c$  was also inferred for two other similar cells (efficiency of 19.01% and 19.12%) to be 1.08 and 3.53  $\text{m}\Omega\text{-cm}^2$ , respectively. The average and standard deviation of  $\rho_c$  for all three cells is then  $3.3 \pm 2.1 \text{ m}\Omega\text{-cm}^2$ . Note that (3) is valid provided  $w/2 < L_T$ , where  $L_T$  is the current transfer length given by  $(\sqrt{\rho_c R_{sheet}})$  [5]. This requirement is met for the average contact resistivity ( $40 \mu\text{m} < 55 \mu\text{m}$ ).

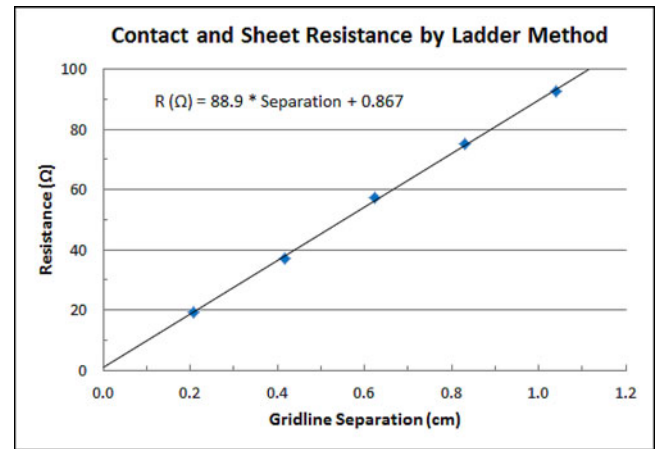


Fig. 4. Resistance data for determining contact resistivity (3.51  $\text{m}\Omega\text{-cm}^2$ ) and sheet resistance (88.9  $\Omega/\square$ ) directly from a TLM-type pattern for 19.12% cell.

In order to check the validity of the inferred contact resistivity, a TLM-like pattern was laser cut from the 19.12% cell, which had an inferred  $\rho_c$  of 3.53  $\text{m}\Omega\text{-cm}^2$ . The test pattern was a strip, 1.00 cm wide, cut perpendicular to the gridlines. The test strip has the appearance of a ladder, with the gridline segments forming the rungs of the ladder and acting as the contact bars in a TLM pattern. Center-to-center spacing of the gridlines was 0.208 cm. As described in [6], the resistance is measured from a reference line to lines 1, 2, 3, 4, and 5 spacings removed from that reference line. A plot of such measured resistances as a function of gridline separation is given in Fig. 4, along with the equation for the fitted line. Since the width of the test pattern is 1.00 cm, the slope of the line gives the emitter sheet resistance as 88.9  $\Omega/\square$ . The intercept (0.867  $\Omega$ ) represents the contact resistance for two bars or gridlines. With the gridline width measured as 81  $\mu\text{m}$  and length as 1.00 cm, the contact resistivity measured directly by this TLM-ladder method is given as follows:

$$\rho_c = \frac{1}{2} * 0.867 \Omega * 0.0081 \text{ cm} * 1.00 \text{ cm} = 3.51 \text{ m}\Omega \cdot \text{cm}^2. \quad (4)$$

This direct measurement of  $\rho_c$  ( $3.51 \text{ m}\Omega\cdot\text{cm}^2$ ) agrees remarkably well with the inferred value ( $3.53 \text{ m}\Omega\cdot\text{cm}^2$ )—in fact, considerably better than an error analysis would indicate.

It should be appreciated that the inferred  $r_s$ (contact) of (2) is small compared with  $r_s$ (total) in a well-designed cell, and is calculated based on a number of measured parameters, each of which has an uncertainty (error). An error analysis was carried out based on standard deviations from five to ten measurements of the required parameters (except for  $\rho_w$ ), according to [9]. The parameters used, along with their standard deviations, are:  $V_{oc}$  of  $0.6410 \pm 0.00012 \text{ V}$ ,  $J_{sc}$  of  $37.80 \pm 0.011 \text{ mA/cm}^2$ , FF of  $0.7869 \pm 0.00126$ , PFF of  $0.830 \pm 0.00045$ , BBR of  $0.056 \pm 0.00142 \Omega$ ,  $R_{sheet}$  of  $91 \pm 3.89 \Omega/\square$ , and  $\rho_w$  of  $2 \pm 1 \Omega\cdot\text{cm}$ . Equations (1) and (2) then yielded a value of  $r_s$ (contact) of  $0.139 \pm 0.037 \Omega\cdot\text{cm}^2$ , or  $0.139 \Omega\cdot\text{cm}^2 \pm 27\%$ . Contributions to the uncertainty were comparable (within a factor of 3) from the cell parameters of (1), BBR,  $R_{sheet}$ , and  $\rho_w$ . Allowing a  $w$  value of  $80 \pm 10 \mu\text{m}$  to propagate through  $f$ ,  $\rho_c$  is determined from (3) to be  $5.27 \pm 1.55 \text{ m}\Omega\cdot\text{cm}^2$ , or  $5.27 \text{ m}\Omega\cdot\text{cm}^2 \pm 29\%$ . Thus, the error analysis suggests the inferred contact resistivity is valid to within  $\pm 1.55 \text{ m}\Omega\cdot\text{cm}^2$ .

#### IV. OPTIMIZING GRIDLINE SPACING FOR MAXIMUM EFFICIENCY OR FOR MINIMUM COST

With material and geometric contact properties having been measured for a real cell fabricated with current technology, it is now possible to optimize gridline spacing to either maximize efficiency or minimize incremental cost ( $\Delta\$/W$ ) of the front silver grid. Recall that measurements from the previous section indicated a postfiring silver gridline width of  $80 \mu\text{m}$ . By knowing the weight of the silver paste used to print the front contact (gridlines and busbars) and the fraction of the paste weight attributable to silver (typically 85%), the average thickness of the printed silver is calculated to be  $7.4 \mu\text{m}$ . By further knowing the BBR value, the effective resistivity of the printed silver gridlines is calculated to be  $4.7 \mu\Omega\cdot\text{cm}$  (three times the bulk value of  $1.59 \mu\Omega\cdot\text{cm}$ ). The gridline material property (effective resistivity) and geometrical properties (width and average thickness), which have been demonstrated for current screen-printing technology and silver paste composition, remain constant as the spacing between gridlines is varied in an optimization calculation, as does the emitter sheet resistance ( $91 \Omega/\square$ ) and the associated contact resistivity ( $5.3 \text{ m}\Omega\cdot\text{cm}^2$ ).

The results are given in Fig. 5. For these calculations, the cost of the silver paste is assumed to be  $\$1/\text{g}$ , representative of current prices which are dominated by the cost of silver. The cost axis of Fig. 5 ( $\Delta\$/W$ ) is associated with the front silver contact system only, and takes into account the cost of the material (silver paste) and the distribution of that material in the contact pattern (number of gridlines and busbars). Fig. 5 indicates that the minimum cost of the front silver contact is  $\$0.038/W$  at an efficiency of 19.0% with a line spacing of 0.21 cm (74 lines), while the maximum efficiency is 19.1% at a cost of  $\$0.040/W$  with a line spacing of 0.17 cm (91 lines). Note that the cell analyzed in the previous section has 74 lines, which is consistent with a contact system designed to minimize the incremental cost

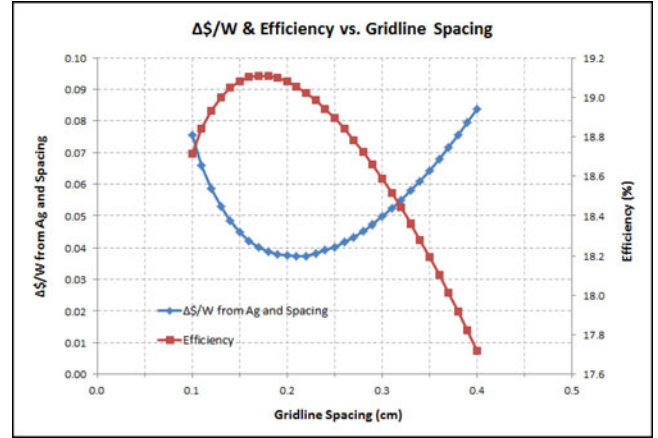


Fig. 5. Plot of calculations to determine gridline spacing to maximize efficiency (0.17 cm, 91 lines) or minimize cost (0.21 cm, 74 lines). Gridline width, thickness, and resistivity are held constant at  $80 \mu\text{m}$ ,  $7.4 \mu\text{m}$ , and  $4.7 \mu\Omega\cdot\text{cm}$  in the calculations. Cost of silver paste is assumed to be  $\$1/\text{g}$ .

per Watt. This analysis shows that a marginally higher efficiency (0.1% absolute) can be obtained at an increased expense of  $\$0.002/W$  for the additional silver material. Although higher efficiency is desirable, and can sometimes command a premium price, it is unlikely that the market would be willing to pay an extra  $\$0.002/W$  for an added 0.1% in absolute efficiency.

In the efficiency calculation for Fig. 5, the impact of gridline spacing on FF  $J_{sc}$  and  $V_{oc}$  is taken into account. As this spacing increases, FF decreases by virtue of increased series resistance, while  $J_{sc}$  increases because of reduced shadowing.  $V_{oc}$  increases with increased spacing because of reduced recombination at the overall metal/silicon interface. As described in [10]

$$J_0 = J_{0b} + (f)(J_{0e-\text{met}}) + (1 - f)(J_{0e-n+}) \quad (5)$$

where  $J_0$  is the total reverse saturation current density,  $f$  is the fraction of the cell surface covered with gridlines (e.g., 0.0379 at 2.10-mm spacing),  $J_{0e-\text{met}}$  is the  $J_0$  component associated with the metallized emitter surface and its underlying  $n^+$  region (taken to be  $1500 \text{ fA/cm}^2$  as a representative value from [10]),  $J_{0e-n+}$  is the  $J_0$  component associated with the unmetallized emitter surface and its underlying  $n^+$  region (taken to be  $60 \text{ fA/cm}^2$  from Suniva measurements), and  $J_{0b}$  is the  $J_0$  component associated with the full base, including the fully metallized back surface field region (taken to be  $450 \text{ fA/cm}^2$  based on Suniva measurements and on [11]).

In order to place cell performance on a firm footing, another  $p$ -base cell fabricated according to the process outlined above was sent to Fraunhofer ISE CalLab for certification. Results for this 156-mm pseudosquare cell are given in Fig. 6, showing a confirmed stabilized efficiency of 19.05% with  $I_{sc}$  of  $9.019 \text{ A}$  ( $J_{sc}$  of  $37.67 \text{ mA/cm}^2$ ),  $V_{oc}$  of  $0.6397 \text{ V}$ , and FF of 0.7903. This cell had 74 gridlines and was fabricated according to the minimum silver cost guidelines.

#### V. CONSIDERATION OF FUTURE TRENDS

The methodology that has been developed can be applied to examine the impact of the cost of silver paste and gridline

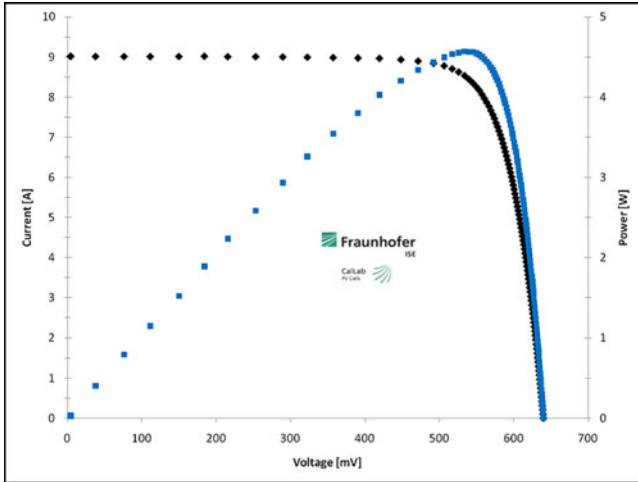


Fig. 6. Fraunhofer-certified 19.05% cell (Suniva cell SUN\_SEL\_8).

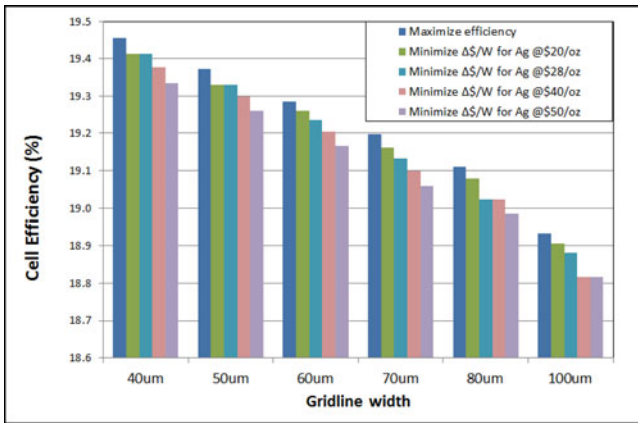


Fig. 7. Calculated cell efficiency resulting from optimizing gridline spacing to either maximize efficiency or minimize silver cost, with silver cost and gridline width as parameters. (Troy Ounce is abbreviated as oz.)

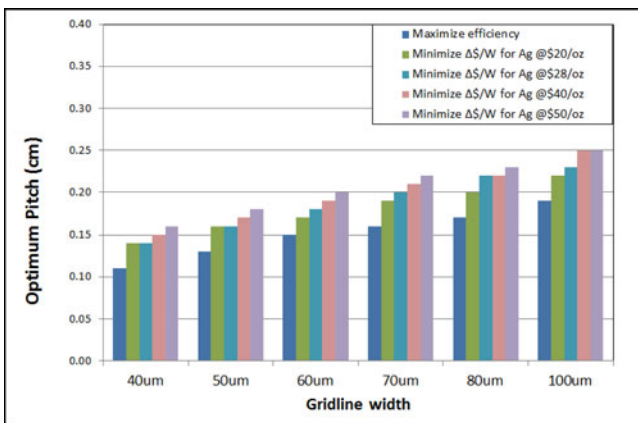


Fig. 8. Calculated gridline spacing to either maximize efficiency or minimize silver cost with silver cost and gridline width as parameters. (Troy Ounce is abbreviated as oz.)

width on cell efficiency and on gridline spacing. Figs. 7 and 8 summarize the results of one such analysis. In all cases, the values of average gridline thickness ( $7.4 \mu\text{m}$ ), gridline width ( $80 \mu\text{m}$ ), effective gridline resistivity ( $4.7 \mu\Omega\cdot\text{cm}$ ), contact resistivity ( $5.3 \text{ m}\Omega\cdot\text{cm}^2$ ), and emitter sheet resistance ( $91 \Omega/\square$ )

that were extracted from measurements and analysis of a fabricated cell were used. In Figs. 7 and 8, Troy Ounce is abbreviated as oz, where 1 oz is equivalent to 31.1 g. Note that as silver prices go up, efficiency decreases (see Fig. 7) and gridline spacing increases (see Fig. 8) in order to minimize  $\Delta S/W$ . Maximum efficiency is independent of silver cost and favors narrow gridlines with small spacing, as expected.

## VI. CONCLUSION

From this paper, the following conclusions can be drawn.

- 1) Accurate analysis of the gridline loss component in an H-bar contact grid system is greatly facilitated by a simple measurement of busbar-to-busbar resistance.
- 2) The proper treatment of current arriving at a busbar from discrete gridlines gives a series resistance component for the busbar, which is a factor of  $[(n+1)(n+2)]/n^2$  larger than that given assuming a continuous flow of current into the busbar, where  $n$  is the number of gridlines per current probe.
- 3) Contact resistivity of the front silver contact can be inferred from the measurement of pseudo FF ( $S_{\text{uns}} - V_{\text{oc}}$ ), cell  $J_{\text{sc}}$ ,  $V_{\text{oc}}$ , and FF ( $I-V$  curve) and the determination of six components of series resistance along with the fractional area covered—without resorting to a TLM measurement.
- 4) Error analysis suggests inferred contact resistivity is accurate to within approximately  $\pm 1.6 \text{ m}\Omega\cdot\text{cm}^2$ .
- 5) Current screen-printing technology and silver paste allow for a contact resistivity of approximately  $3.3 \text{ m}\Omega\cdot\text{cm}^2$  when contacting a  $90 \Omega/\square$  ion implanted/annealed phosphorus-doped emitter.
- 6) Current screen-printing technology and silver paste cost indicate gridline spacing of 1.7 mm to maximize efficiency and 2.1 mm to minimize silver cost.
- 7) Guidance regarding optimum gridline spacing (screen design), which follows from future silver price changes or lifting of technological limits (gridline width) is available through a contact analysis, as described.
- 8) Contact analysis helps to enable full-sized ( $239 \text{ cm}^2$ ) production-worthy cells fabricated from p-Cz silicon substrates with efficiencies in excess of 19%, as confirmed by Fraunhofer ISE CaLab.

## ACKNOWLEDGMENT

The authors gratefully acknowledge the Suniva production staff and the Suniva R&D staff for their assistance in processing the cells used in this study.

## REFERENCES

- [1] M. Wolf, "Metallization for large-area solar cells," in *Proc. 15th Photovoltaic Spec. Conf.*, 1981, pp. 506–511.
- [2] L. J. Caballero, P. Sanchez-Friera, B. Lalajuna, J. Alonso, and M. A. Vazquez, "Series resistance modeling of industrial screen-printed monocrystalline silicon solar cells and modules including the effect of spot soldering," in *Proc. 4th World Conf. Photovoltaic Energy Convers.*, 2006, pp. 1388–1391.

- [3] L. J. Caballero, A. Martinez, P. Sanchez-Friera, M. A. Vazquez, and J. Alonso, "Front grid design in industrial silicon solar cells: Modelling to evaluate the behaviour of three vs. two buses cell patterns," in *Proc. 33rd Photovoltaic Spec. Conf.*, 2008, pp. 1–4.
- [4] L. J. Caballero, "Contact definition in industrial silicon solar cells," in *Solar Energy*, Rijeka, Croatia: Intech, 2010, ch. 16, pp. 375–398.
- [5] D. L. Meier and D. K. Schroder, "Contact resistance: Its measurement and relative importance to power loss in a solar cell," *IEEE Trans. Electron Devices*, vol. 31, no. 5, pp. 647–653, May 1984.
- [6] D. L. Meier, E. A. Good, R. A. Garcia, B. B. Bingham, S. Yamanaka, V. Chandrasekaran, and C. Bucher, "Determining components of series resistance from measurements on a finished cell," in *Proc. 4th World Conf. Photovoltaic Energy Convers.*, May 2006, pp. 1315–1318.
- [7] R. A. Sinton, A. Cuevas, and M. Stuckings, "Quasi-steady-state photoconductance: A new method for solar cell material and device characterization," in *Proc. 25th Photovoltaic Spec. Conf.*, May 1996, pp. 457–460.
- [8] A. L. Fahrenbruch and R. H. Bube, *Fundamentals of Solar Cells*, New York: Academic, 1983, pp. 220–222.
- [9] P. R. Bevington, *Data Reduction and Error Analysis for the Physical Sciences*, New York: McGraw-Hill, 1969, pp. 56–65.
- [10] T. Fellmeth, A. Born, A. Kimmerle, F. Clement, D. Biro, and R. Preu, "Recombination at metal emitter interfaces of front contact technologies for highly efficient silicon solar cells," *Energy Procedia*, vol. 8, pp. 115–121, 2011.
- [11] R. Woehl, P. Gundel, J. Krause, K. Rühle, F. D. Heinz, M. Rauer, C. Schmiga, M. C. Schubert, W. Warta, and D. Biro, "Evaluating the aluminum-alloyed p<sup>+</sup>-layer of silicon solar cells by emitter saturation current density and optical microspectroscopy measurements," *IEEE Trans. Electron Devices*, vol. 58, no. 2, pp. 441–447, Feb. 2011.



**Daniel L. Meier** (M'08) received the B.S. degree in physics from St. Vincent College, Latrobe, PA, in 1969 and the M.S. degrees in physics in 1971 and in measurement and control in 1978, and the Ph.D. degree in solid state physics in 1976, from Carnegie-Mellon University (CMU), Pittsburgh, PA.

After spending four years in the field of ocean thermal energy conversion at CMU, he began his career in photovoltaics in 1980 with the Westinghouse Electric Corporation. Over the years, he has held a variety of scientific and executive positions with Westing-

house, EBARA Solar, Solar Power Industries, the National Renewable Energy Laboratory, and Suniva, Norcross, GA – most recently as Chief Scientist with Suniva. After leaving Suniva in 2012, he founded Lightdrop Harvest, LLC, St. Marys, PA, to offer consulting services to the photovoltaics community. He has published over 90 technical papers and has been granted 13 U.S. patents. His research interests include the design, fabrication, and characterization of production-worthy silicon solar cells and modules, with emphasis on junction formation by ion implantation and on contact systems.

**Vinodh Chandrasekaran** (M'12) received the B.E. degree in electronics and communication engineering from the University of Madras, Chennai, India, in 2002 and the M.S.E.E. degree from the University of South Florida, Tampa, specializing in thin-film photovoltaics, in 2005.

He is currently a Senior R&D Engineer with Suniva, Norcross, GA, where he is primarily responsible for development of contacts to advanced cell structures and cost reduction. He has also been focused on the development and transfer of technology from the lab, achieving cell efficiency levels of more than 19% in production. Prior to joining Suniva, he was with Solar Power Industries, where he worked on the development and manufacturing of multicrystalline silicon solar cells. He was also involved in multicrystalline ingot growth and the wire sawing process.



**Atul Gupta** received the B.S. degree in chemical engineering from the Indian Institute of Technology, Delhi, in 1996, two M.S. degrees in chemical and electrical and computer engineering in 1999 and 2000, respectively, and the Ph.D. degree in chemical engineering in 2001, all from North Carolina State University, Raleigh.

He has been with Suniva, Norcross, GA, since 2011, where he is currently the Director of Product Development and R&D. He has several papers in this field and has been awarded 20 patents. He has held

several positions of increasing responsibility since 2001, starting his industry career at the R&D headquarters of Advanced Micro Devices, where his primary responsibility was developing and transferring new processes and technologies in thin-film deposition for complementary metal-oxide semiconductor device (logic and flash memory) manufacturing. He then joined Varian Semiconductor Equipment as principal engineer, where he was responsible first for developing a plasma doping implanter and then was instrumental in creating a new business unit focused on developing an implanter for solar cell manufacturing. His primary responsibilities include the development and deployment of new cell structures that meet industry leading high-efficiency and lower cost objectives for Suniva, in addition to managing the intellectual property portfolio for Suniva.

**Vijay Yelundur** received the B.S. and the Ph.D. degrees in materials science and engineering from the Georgia Institute of Technology (Georgia Tech), Atlanta, in 1997 and 2003, respectively.

He is currently Manager of the Manufacturing Innovation Center, Suniva, Norcross, GA, where he is involved with low-cost c-Si cell technology development and transfer into manufacturing. He joined Suniva after five years as a Senior Research Engineer with the University Center of Excellence for Photovoltaics Research and Education at Georgia Tech, where his research interests included process integration for high-efficiency manufacturable c-Si solar cells and the gettering and passivation of defects in low-cost Si materials. He has published more than 30 technical papers in the field of c-Si photovoltaics.



**Ajeet Rohatgi** (F'08) received the B.S. degree in electrical engineering from the Indian Institute of Technology, Kanpur, India, in 1971, the M.S. degree from Virginia Tech, Blacksburg, in 1973, and the Ph.D. degree in metallurgy and material science from Lehigh University, Bethlehem, PA, in 1977.

He is currently a Regents' Professor and a Georgia Power Distinguished Professor with the School of Electrical Engineering, Georgia Institute of Technology (Georgia Tech), Atlanta. In 2007, he founded Suniva, Inc., Norcross, GA, to manufacture silicon

solar cells and modules that are situated at the right intersection of cost and efficiency, where he is the Chief Technology Officer. He is also the founding director of the University Center of Excellence for Photovoltaic Research and Education, Georgia Tech. He has published more than 400 technical papers in this field and has been awarded 15 patents. As part of the 1996 Olympics in Atlanta, he and his group designed and installed the world's largest grid-connected, roof-top photovoltaic (PV) system on the Georgia Tech Aquatic Center. His current research interests include the development of cost and efficiency roadmaps for attaining grid parity with Silicon PV, understanding of impurity effects in silicon solar cells, gettering and passivation of defects in solar grade silicon, ion implantation and rapid thermal processing of solar cells, the design and fabrication of high-efficiency commercial ready n- and p-base silicon solar cells, and the economics of PV systems.

Dr. Rohatgi received the Westinghouse Engineering Achievement Award in 1985, the Distinguished Professor Award from Georgia Tech in 1996, the IEEE PVSC William Cherry Award in 2003, the Climate Protection Award from the Environmental Protection Agency, and the Outstanding Educator and Innovator Award in PV from the American Solar Energy Society in 2009. In 2010, he was named one of the Champions of PV by *Renewable Energy World* magazine.